ELSEVIER

International Journal of Solids and Structures 41 (2004) 3625–3641

INTERNATIONAL JOURNAL OF SOLIDS and STRUCTURES

www.elsevier.com/locate/ijsolstr

Modelling in-plane micro-structure of masonry walls by rigid elements

Siro Casolo *

Dipartimento di Ingegneria Strutturale, Politecnico di Milano, Piazza Leonardo da Vinci 32, 20133 Milano, Italy

Received 10 April 2003; received in revised form 23 January 2004
Available online 10 March 2004

Abstract

This paper proposes rigid elements for a specific simplified model of the in-plane behaviour of masonry walls made of regular textures. The elements are plane, quadrilateral and connected by two normal springs and one shear spring on each side. The mechanical characteristics of these connections are defined in consideration of the texture effects arising due to the mechanical degradation of mortar. The present approach has proved effective when transferring the essential texture information from micro-scale to macro-scale. In particular, the "local rotation" of the blocks is obtained by assigning different stiffness to the shear springs, according to their orientation, while the in-plane bending stiffness can be reproduced by properly disposing the two normal springs. Depending on the geometry of the textures, these aspects are significant in case of large differences in the elastic modulus of the constituents, as is the case of masonry walls subjected to heavy seismic loading. Numerical simulations have proved that it is possible to deal with these aspects with a very reduced computational effort which is promising for non-linear dynamical analyses applications.

Keywords: Rigid elements; Masonry texture; Micro-structure; Local rotation

1. Introduction

When studying the response of buildings subjected to earthquakes, it is necessary to describe the dynamical response of large portions of structures with respect to the effects of a number of varying parameters. As a consequence, specific computational models are required; on the one hand these models should be simplified enough to allow parametric full dynamical analyses, on the other hand they should also account for the peculiar behaviour of masonry material under loading causing heavy mechanical degradation. Moreover, when dealing with structural intervention on ancient masonry monuments the presence of complex different textures must often be considered, e.g. Fig. 1. The present study focuses on the numerical approximation of the in-plane behaviour of the two idealized composite "masonry-like" textures shown in Fig. 2. The geometry of a standard Italian brick has been adopted for the rectangular

* Tel.: +39-02-2399-4356; fax: +39-02-2399-4220.
E-mail address: siro.casolo@polimi.it (S. Casolo).

0020-7683/$ - see front matter © 2004 Elsevier Ltd. All rights reserved.
doi:10.1016/j.ijsolstr.2004.02.002

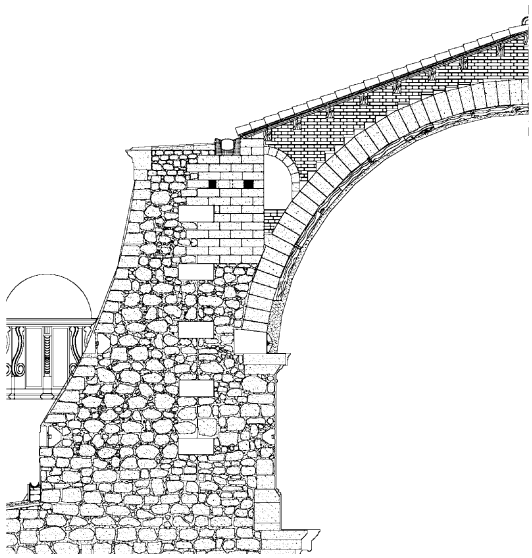

Fig. 1. Partial section of an arch of the nave of an ancient cathedral, Italy.

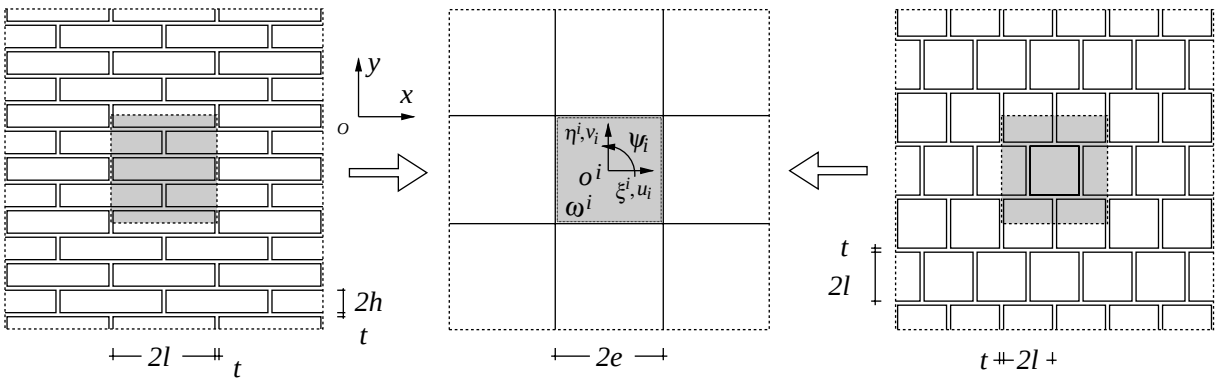

Fig. 2. Scheme of two masonry-like textures; a common rigid element discretization is shown in the centre.

block texture: $2l \times 2h = 25 \times 5.5$ cm^2, whereas for square blocks the side is assumed to be $2l = 12$ cm. The thickness of the mortar joints is $t = 1$ cm. The vertical head-joints, which are interrupted by bricks, are generally of poor quality and weaker than the horizontal continuous bed-joints. For the sake of clarity single leaf masonry has been considered as a first approach.

Dealing with composites, discrete models with a reduced number of degrees of freedom can be obtained by adopting a formulation in which the mechanical characteristics of heterogeneous materials are averaged by means of homogenization towards an equivalent elastic medium (Anthoine, 1995; Michel et al., 1999; Pande et al., 1989; Zucchini and Lourenço, 2002). Unfortunately, a lot of information about micro-structure tends to get lost in a similar process, while there are, however, cases where the relevance of the micro-structure effects should not be completely neglected, depending on global geometry, texture, the size of the blocks with respect to the size of the structure, and the different stiffness of the material components. In order to retain some of the micro-structure information in the passage from micro-scale to macro-scale,

it is possible to homogenize towards a generalized continuum. As an example, finite element models that adopt a Cosserat continuum have been proposed when using rigid blocks, or in case of materials which show strain softening and the localization of deformation (Bouyge et al., 2001; Masiani et al., 1995; Mühlhaus, 1989; Sulem and Mühlhaus, 1997; van der Sluis et al., 1999; Trovalusci and Masiani, 1999). Unfortunately, applying such refined theories to simplified computational models still causes some trouble, because of the difficulty in defining a clear and simple procedure for assigning the elastic–plastic parameters and the characteristic length.

In the field of dynamical analysis, it is well known that rigid element models are powerful and effective, as they require very few degrees of freedom to approximate the fundamental modes of vibration (Kawai, 1978; Toy and Yoshida, 1991). Adopting a proper constitutive relation, this approach has been successfully applied to the out-of-plane dynamical analysis of masonry walls characterized by non-linearity and mechanical degradation of the material (Casolo, 1999, 2000). The present paper proposes the application to the in-plane analysis of structural elements for which texture effects are significant, by adopting quadrilateral elements which are on each side connected by three elastic devices that may be imagined as simple linear springs. The adoption of this type of device is useful in view of future developments, since it allows separate phenomenological descriptions for the hysteresis behaviour of the axial and shear connections that can be related by means of a simple Mohr-Coulomb criterion. By imposing the strain energy equivalence, the mechanical characteristics of the model are defined by means of a specific identification procedure with the objective of transferring the "memory" of the texture to the element's meso-scale by exploiting the peculiar rigid element kinematics.

2. Model discretization

The in-plane kinematics of the structure is defined by its mid-plane $\Omega \subset \Re^2$, and a global Cartesian coordinate frame $\{O, x, y\}$ is fixed with the x-axis parallel to the horizontal bed-joints. The domain Ω is then partitioned into m quadrilateral elements ω^i so that no vertex of one quadrilateral lies on the edge of another quadrilateral. A local reference frame $\{o^i, \xi^i, \eta^i\}$ is placed in each element barycentre o^i, where ξ^i-axis is initially parallel to the global x-axis as shown in Fig. 2. The deformed configuration of the discrete model is described as a function of the displacement of these local reference frames fixed to the moving elements. Three kinematic variables, the two translations u_i, v_i and the rotation angle ψ_i, are associated to each element as shown in Fig. 3, and the whole kinematic configuration is described by the $3m$ Lagrangian coordinates assembled in the vector $\{u\}$:

$$\{u\}^{\mathrm{T}} = \{u_1, v_1, \psi_1, u_2, v_2, \psi_2, \ldots, u_m, v_m, \psi_m\} \tag{1}$$

The external load, including inertial forces, is applied considering the undeformed geometry. For each element ω^i, it is condensed into three resultants: the horizontal and the vertical forces p_i and q_i, applied to the barycentre o^i, and the couple μ_i. The m triplets $\{p_i, q_i, \mu_i\}$ are assembled into a vector of generalized external load $\{p\}$, conjugated with vector $\{u\}$, as follows:

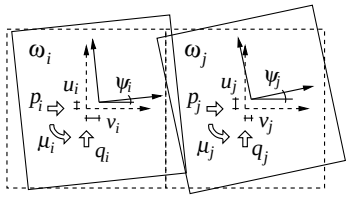

Fig. 3. Displaced couple of rigid elements with evidence of the notation adopted for the displacements and external forces.

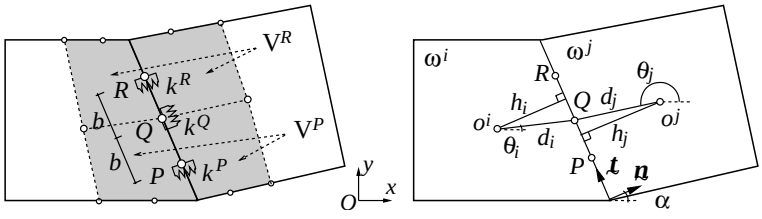

Fig. 4. Couple of rigid elements ω^i and ω^j of irregular shape with evidence of the tributary volumes V^R and V^P and the notation adopted for the elastic devices.

$$\{p\}^{\mathrm{T}} = \{p_1, q_1, \mu_1, p_2, q_2, \mu_2, \ldots, p_m, q_m, \mu_m\} \tag{2}$$

The elastic devices that connect each couple of elements are placed in correspondence of three connection points named P, Q and R, as shown in Fig. 4, on the left, where the shaded areas indicate the volumes of pertinence V^P, V^R and $\mathrm{V}^Q = \mathrm{V}^P + \mathrm{V}^R$, associated to each of these points. A *shear elastic connection* is placed in the mid-point Q, while two *normal elastic connections* are placed at the external points P and R, at the distance b from Q. The elastic force in each device is proportional to a mean strain measure associated with the corresponding connection point: a shear strain ε^Q is associated with point Q, while axial strains ε^P and ε^R, are associated with points P and R. The corresponding *local generalized stiffnesses* are named k^P, k^Q, k^R. Given the distances d_i and d_j of the two baricentres from point Q, and the distances h_i and h_j of the two baricentres from the connection side, as shown in Fig. 4, on the right, and assuming small displacements, the following relation gives the three strain measures between a couple of adjoining elements ω^i and ω^j, as a function of the Lagrangian coordinates $\{u\}$:

$$\begin{Bmatrix} \varepsilon^P \\ \varepsilon^Q \\ \varepsilon^R \end{Bmatrix} = -\frac{1}{h_i + h_j} \begin{bmatrix} \cos\alpha & \sin\alpha & [\sin(\alpha-\theta_i)d_i + b] \\ -\sin\alpha & \cos\alpha & [\cos(\alpha-\theta_i)d_i] \\ \cos\alpha & \sin\alpha & [\sin(\alpha-\theta_i)d_i - b] \end{bmatrix} \begin{Bmatrix} u_i \\ v_i \\ \psi_i \end{Bmatrix} + \frac{1}{h_i + h_j} \begin{bmatrix} \cos\alpha & \sin\alpha & [\sin(\alpha-\theta_j)d_j + b] \\ -\sin\alpha & \cos\alpha & [\cos(\alpha-\theta_j)d_j] \\ \cos\alpha & \sin\alpha & [\sin(\alpha-\theta_j)d_j - b] \end{bmatrix} \begin{Bmatrix} u_j \\ v_j \\ \psi_j \end{Bmatrix} \tag{3}$$

The vector of *generalized strains* $\{\varepsilon\}$ is assembled in order to contain all the mean strain measures as follows:

$$\{\varepsilon\}^{\mathrm{T}} = \{\varepsilon_1^P, \varepsilon_1^Q, \varepsilon_1^R, \varepsilon_2^P, \varepsilon_2^Q, \varepsilon_2^R, \ldots, \varepsilon_r^P, \varepsilon_r^Q, \varepsilon_r^R\} \tag{4}$$

being r the number of sides that connect the elements of the whole discrete model. Thus, the linearity of (3), permits to express the strain-displacement relations by considering a $3r \times 3m$ matrix $[B]$:

$$\{\varepsilon\} = [B]\{u\} \tag{5}$$

3. Constitutive relations

3.1. Direct numerical identification

The mechanical characteristics of the connecting devices are assigned with the criterion of approximating the strain energy of the corresponding volume of pertinence by means of a direct numerical identification (Anthoine, 1995; Bouyge et al., 2001; Michel et al., 1999). The five loading tests shown in Fig. 5 are per-

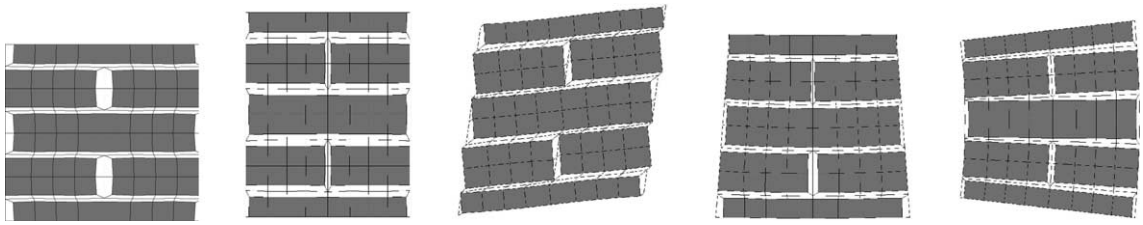

Fig. 5. Sketch of the five loading tests performed on a periodic cell.

formed adopting a plane stress finite element model of the periodic cell as reference, and assigning periodic boundary conditions for axial and shear loading, and displacement boundary conditions for in-plane bending. The corresponding average strain energy densities evaluated by finite elements are named respectively $\mathscr{U}_x^A$, $\mathscr{U}_y^A$, $\mathscr{U}^S$, $\mathscr{U}_x^F$ and $\mathscr{U}_y^F$. For the sake of clarity, the method is presented with reference to the case of a regular mesh of square rigid elements aligned with the principal axes of the material, whose size corresponds to the side $2e$ of a square periodic cell, as shown in Fig. 2.

The axial behaviour is characterized by equal actions in the two normal connecting devices of the common side as shown in Fig. 6. Noting that the present model cannot account for the Poisson coupling effect, the choice of considering free normal displacements on the boundary sides without load has been assumed in the present case. The generalized axial strains are $\varepsilon_x = u/e$ and $\varepsilon_y = v/e$, while the measured strain energy densities, averaged in the volumes of pertinence, are $\mathscr{U}_x^A$ and $\mathscr{U}_y^A$. Thus, the generalized axial stiffnesses per unit volume to be attributed to the normal connecting devices, $k_x^A = k_x^P = k_x^R$ and $k_y^A = k_y^P = k_y^R$, are calculated as follows:

$$k_x^A = \frac{2\mathscr{U}_x^A}{\varepsilon_x^2}, \quad k_y^A = \frac{2\mathscr{U}_y^A}{\varepsilon_y^2} \tag{6}$$

The shear behaviour is characterized by the presence of equal forces in the shear connecting devices of the four sides of each square element. Finite element analyses carried out on the two idealized "masonry-like" textures have revealed a significant difference in the deformation patterns, as shown, for example, in Fig. 7. In fact, rectangular blocks tend to rotate so as to align the long side with the horizontal joints, whereas square blocks tend to translate without significant rotation. In detail, the deformation of rectangular blocks appears as a mix of shear and bending, plus a local rigid rotation, as reported in Fig. 8 which

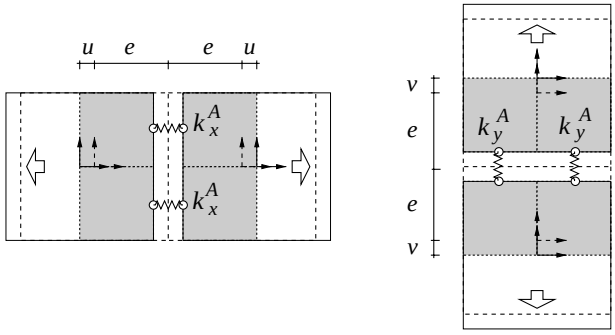

Fig. 6. Couple of rigid elements subjected to horizontal and vertical axial loading.

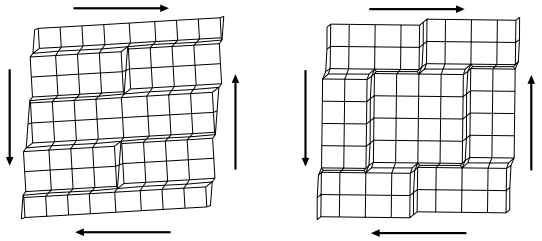

Fig. 7. Enlarged view of the deformed finite element mesh of a periodic cell of the two textures subjected to shear loading.

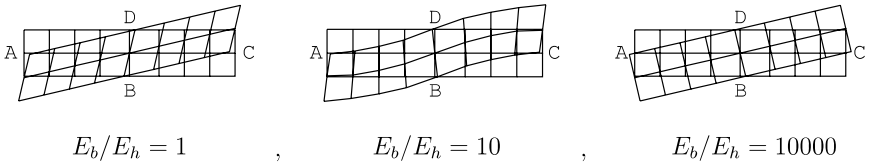

Fig. 8. Deformed shapes of a block with different ratios of elastic moduli E_b/E_h.

shows the enlarged images of the central brick in correspondence with three different ratios of the elastic modulus of the bricks E_b with respect to the elastic modulus of the horizontal and vertical mortar joints, respectively E_h and E_v (in this case $E_h/E_v = 10$). We can observe that the brick responds with a pure shear deformation for $E_b/E_h = 1$, with a mix of shear and bending for $E_b/E_h = 10$, while rigid rotation prevails for $E_b/E_h = 10\,000$. This very high ratio has been considered in order to investigate the condition of plastic loading when mortar degrades. The rigid rotation of the blocks can be considered as a characteristic *local rotation* of this masonry-like texture, and its importance eventually increases with the level of heterogeneity. Fig. 9 shows the shear case with reference to an assemblage of four rigid elements, and the shaded area corresponds to half of the volume of pertinence of the four shear connecting devices. The average symmetric shear strain is $\varepsilon_s = u/e = v/e$, while the local rotation is reproduced by exploiting the rotation degree of freedom of the rigid elements. In particular, by adopting square rigid elements whose size is $2e$, the local rigid rotation of the blocks can be directly assigned as the rotation ψ of the rigid elements. The proper

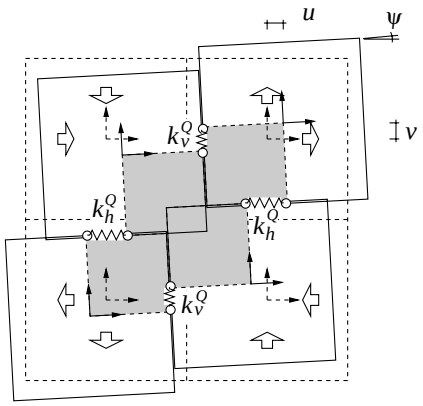

Fig. 9. Assemblage of four rigid elements subjected to shear loading.

measure of this local rotation is in some way a compromise since it tends to be affected by shear and bending deformation. At the present stage, the following formula has been chosen, based on the displacements of the points A, B, C and D of the brick shown in Fig. 8:

$$\psi = \frac{u_y^C - u_y^A}{4l} + \frac{u_x^D - u_x^B}{4h} \tag{7}$$

The generalized shear strains for vertical and horizontal connecting devices are:

$$\begin{aligned} \varepsilon_{\mathrm{v}} &= \varepsilon_{\mathrm{s}} - \psi = \varepsilon_{\mathrm{s}}(1-\rho) \\ \varepsilon_{\mathrm{h}} &= \varepsilon_{\mathrm{s}} + \psi = \varepsilon_{\mathrm{s}}(1+\rho) \end{aligned} \tag{8}$$

being $\rho = \psi/\varepsilon_{\mathrm{s}}$ the *local rigid rotation ratio*. The equilibrium of the shear stresses implies the following relation of stiffnesses of the shear connecting devices of the vertical and of the horizontal sides:

$$\frac{k_{\mathrm{h}}^Q}{k_{\mathrm{v}}^Q} = \frac{\varepsilon_{\mathrm{v}}}{\varepsilon_{\mathrm{h}}} = \frac{1-\rho}{1+\rho} \tag{9}$$

A generalized symmetric shear stiffness k^S can thus be defined, such as:

$$\begin{aligned} (1+\rho)k^S &= k_{\mathrm{v}}^Q \\ (1-\rho)k^S &= k_{\mathrm{h}}^Q \end{aligned} \tag{10}$$

Given the average elastic energy density $\mathscr{U}^S$ stored in the volume of pertinence, as measured by the finite element model, k^S is defined by the following equation:

$$k^S = \frac{\mathscr{U}^S}{(1-\rho^2)\varepsilon_{\mathrm{s}}^2} \tag{11}$$

Modelling the in-plane bending stiffness requires the estimation of the distances b_x and b_y of the normal elastic connections from the mid-point of each side. The scheme of the in-plane bending test is shown in Fig. 10. After measuring the average elastic energy densities $\mathscr{U}_x^F$ and $\mathscr{U}_y^F$ from the finite element model, we obtain:

$$\beta_x = \frac{b_x}{e} = \frac{1}{\psi}\sqrt{\frac{2\mathscr{U}_x^F}{k_x^A}}, \quad \beta_y = \frac{b_y}{e} = \frac{1}{\psi}\sqrt{\frac{2\mathscr{U}_y^F}{k_y^A}} \tag{12}$$

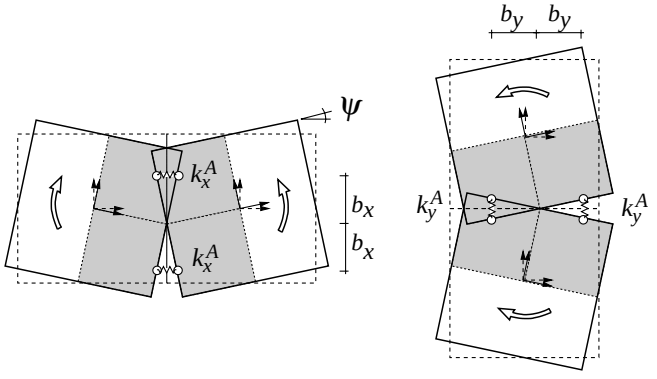

Fig. 10. Couple of rigid elements subjected to in-plane bending.

The case of linear stress distribution along a common side of length $2e$ is simulated by placing the normal connecting devices at $\beta = 1/\sqrt{3} = 0.577$, but in general the value of ratio β varies in order to approximate different stress distribution along the periodic cell sides.

Finally, the generalized stiffnesses per unit volume of all the $3r$ elastic devices and their corresponding volumes of pertinence are assembled in two diagonal matrices $[D]$ and $[V]$ as follows:

$$[D] = \mathrm{Diag}\left\{k_1^P, k_1^Q, k_1^R, k_2^P, k_2^Q, k_2^R, \ldots, k_r^P, k_r^Q, k_r^R\right\} \tag{13}$$

$$[V] = \mathrm{Diag}\left\{V_1^P, V_1^Q, V_1^R, V_2^P, V_2^Q, V_2^R, \ldots, V_r^P, V_r^Q, V_r^R\right\} \tag{14}$$

The three tests for which periodic boundary conditions are assigned are also the basis for defining the elastic properties of a corresponding orthotropic Cauchy continuum for which the local rotation ratio ρ is disregarded. It is worth noting that the generalized strain measures ε_x, ε_y and ε_s defined for rigid elements correspond to the overall strains of an equivalent homogeneous continuum, and thus the following simple equivalence holds between the elastic moduli of the orthotropic Cauchy continuum and the generalized stiffness assigned to the connecting devices, as a consequence of Eqs. (6) and (11): Young's moduli $E_x = k_x^A$, $E_y = k_y^A$, and shear modulus $2G = k^S$.

3.2. Size effects and orientation

In the case of square rigid elements whose size equals the size of the periodic cell then the rotation ψ of rigid elements subjected to pure shear loading coincides with the local rotation measured on the composite material. When the side of the rigid elements is larger than the base side of the blocks, a reduced angle $\psi^* < \psi$ is assigned following the idea that each single element must rotate in order to average the terraced shape of the horizontal joints as shown in Fig. 11. This is done by defining a characteristic length $2f$ for each connecting side as the square root of the area that corresponds to the volume of pertinence of the shear connection. Then length $2f$ is compared with the block base length $2l$, and the reduced ratio $\rho^\star$ between the rotation of the rigid elements and the symmetric shear deformation is assigned as follows:

$$\rho^\star = \begin{cases} \rho l/f & \text{if } f > l \\ \rho & \text{otherwise} \end{cases} \tag{15}$$

being $\rho = \psi/\varepsilon_s$, as defined in Section 3.1.

Using algebra, it can be proved that the approximation of the in-plane bending moment given by Eq. (12) can also be preserved in the case $f > l$ by assigning $b^\star$, the distance of the normal connections, according to the following equation:

$$\beta^\star = \frac{b^\star}{f} = \sqrt{\frac{1}{3} - \frac{l^2}{3f^2} + \frac{b^2}{f^2}} \tag{16}$$

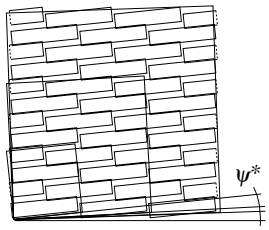

Fig. 11. Example of different rotation angle ψ^* attributed to rigid elements of different size with respect to the periodic square cell.

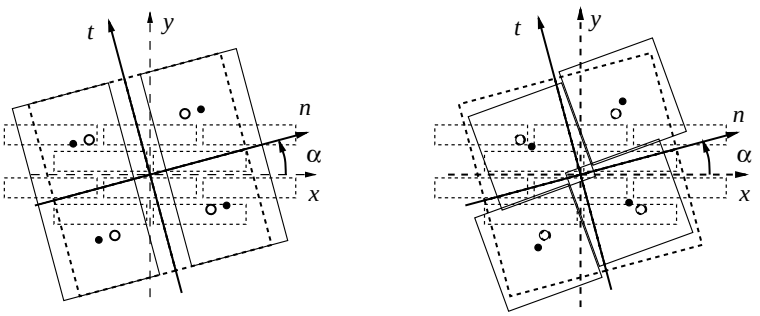

Fig. 12. Inclined meshes subjected to axial strain (left) and shear strain (right).

It is also necessary to specify how to assign the elastic parameters when the normal $\boldsymbol{n}$ of a connecting side is inclined by an angle α with respect to the horizontal x-axis. Considering again square rigid elements, in the case of a deformation map that consists of simple displacements of the element barycentre along the $\boldsymbol{n}$ direction, as shown in Fig. 12 on the left, only the normal elastic connections are interested by a generalized strain ε_n. The corresponding strains in the material reference frame $\{O, x, y\}$ are:

$$\begin{aligned} \varepsilon_x(\alpha) &= \varepsilon_n \cos^2 \alpha \\ \varepsilon_y(\alpha) &= \varepsilon_n \sin^2 \alpha \\ \varepsilon_s(\alpha) &= \varepsilon_n \cos \alpha \sin \alpha \end{aligned} \tag{17}$$

It is worth noting that the presence of the shear strain ε_s in the material reference frame implies an angle of local rotation $\psi(\alpha)$, even if this rotation cannot exist in the inclined mesh:

$$\psi(\alpha) = \rho \varepsilon_s(\alpha) = \rho \varepsilon_n \cos \alpha \sin \alpha \tag{18}$$

Thus, the equivalence of the elastic energy leads to the following expression for the stiffness of the normal connecting devices as a function of angle α:

$$k^A(\alpha) = k_x^A \cos^4 \alpha + k_y^A \sin^4 \alpha + 2k^S(1 - \rho^2) \cos^2 \alpha \sin^2 \alpha \tag{19}$$

In the case of a barycentre deformation map that corresponds to a simple shear strain ε_t, as shown in Fig. 12 on the right, the corresponding strains in the material reference frame $\{O, x, y\}$ are:

$$\begin{aligned} \varepsilon_x(\alpha) &= -2\varepsilon_t \cos \alpha \sin \alpha \\ \varepsilon_y(\alpha) &= 2\varepsilon_t \cos \alpha \sin \alpha \\ \varepsilon_s(\alpha) &= \varepsilon_t(\cos^2 \alpha - \sin^2 \alpha) \end{aligned} \tag{20}$$

The consequent local rotation $\psi(\alpha)$ in the material reference frame is:

$$\psi(\alpha) = \rho \varepsilon_t(\cos^2 \alpha - \sin^2 \alpha) \tag{21}$$

This local rotation can be attributed to the inclined mesh by assigning different stiffness to the shear connecting devices in accordance with Eq. (9). The ratio between local rotation and symmetric shear in the inclined configuration is:

$$\rho^\star(\alpha) = \frac{\psi(\alpha)}{\varepsilon_t} = \rho(\cos^2 \alpha - \sin^2 \alpha) \tag{22}$$

Finally, the equivalence of the elastic energy leads to the following expression for the stiffness of the shear connections as a function of the angle of inclination α:

$$k^S(\alpha) = \frac{2(k_x^A + k_y^A)\cos^2\alpha\sin^2\alpha + k^S(1-\rho^2)(\cos^2\alpha - \sin^2\alpha)^2}{1-\rho(\cos^2\alpha - \sin^2\alpha)} \tag{23}$$

Heuristically, the following simple relation has been assumed for $\beta^\star(\alpha)$:

$$\beta^\star(\alpha) = \beta_x\cos^2\alpha + \beta_y\sin^2\alpha \tag{24}$$

4. Numerical application

4.1. Equations of the motion

The mass of each element m_i and the polar moment of inertia around the barycentre $\imath_i$, are assembled in the following diagonal generalized mass matrix:

$$[M] = \mathrm{Diag}\{m_1, m_1, \imath_1, m_2, m_2, \imath_2, \ldots, m_m, m_m, \imath_m, \} \tag{25}$$

Recalling Eqs. (5), (13) and (14), the global generalized stiffness matrix $[K]$ is:

$$[K] = [B]^{\mathrm{T}}[D][V][B] \tag{26}$$

Thus, the system of equation of the motion of the discrete system is expressed as follows:

$$[M]\{\ddot{u}\} + [K]\{u\} = \{p\} \tag{27}$$

4.2. Elastic parameters related with micro-structure

An extensive parametric study was performed on the textures shown in Fig. 2 in order to identify the mechanical characteristics of the connection devices according to the procedure outlined in Section 3.1. The Young modulus of the blocks was fixed to be $E_{\mathrm{b}} = 10\,000$ MPa, while the elastic moduli of the horizontal and vertical mortar joints, respectively E_{h} and E_{v}, assumed different values. In particular, ratio $E_{\mathrm{b}}/E_{\mathrm{h}}$ varied in the range [1–100 000] while the weakness effect of the vertical joints (Dialer, 1991) was studied by considering four different ratios $E_{\mathrm{h}}/E_{\mathrm{v}}$ in the range [1–30]. Poisson's ratio was fixed to be $\nu = 0.1$ for both materials. Very high $E_{\mathrm{b}}/E_{\mathrm{h}}$ values were considered with the aim of investigating the behaviour during the plastic phases of loading in particular.

Fig. 13 shows the trends of ratios ρ, β_x andβ_y, given by Eqs. (8) and (12), as a function of ratio $E_{\mathrm{b}}/E_{\mathrm{h}}$. The difference in micro-structure behaviour between the two textures is noticeable, and it is worth noting that the rectangular blocks manifest a local counterclockwise rotation ψ that approaches the average symmetric shear strain ε_{s} (i.e. $\rho \to 1$) for high $E_{\mathrm{b}}/E_{\mathrm{h}}$ values, without being significantly influenced by the $E_{\mathrm{h}}/E_{\mathrm{v}}$ ratio. In fact, when mortar has very low stiffness, the elongated shape of the blocks in any case tends to impose the geometric alignment with the bed joints. Square blocks, on the other hand, manifest small values of local rotation that tend to increase clockwise for high $E_{\mathrm{h}}/E_{\mathrm{v}}$ ratios, as a direct consequence of the higher stiffness of the horizontal shear connections with respect to the vertical ones. In practice, with square blocks the effect of the different mortar joint stiffness prevails, while the geometric alignment effect related to the texture is not significant.

The orthotropy of micro-structure effects is evident when considering the in-plane bending stiffness as expressed by parameters β_x and β_y. Along the horizontal direction, the bending stiffness of the rectangular block texture tends to increase at high $E_{\mathrm{b}}/E_{\mathrm{h}}$ values, especially in case of high $E_{\mathrm{h}}/E_{\mathrm{v}}$ ratio values, as manifested by the fact that β_x tends to become larger than 0.577. The behaviour of square block texture is different since the bending stiffness along the horizontal direction does not significantly depend on the

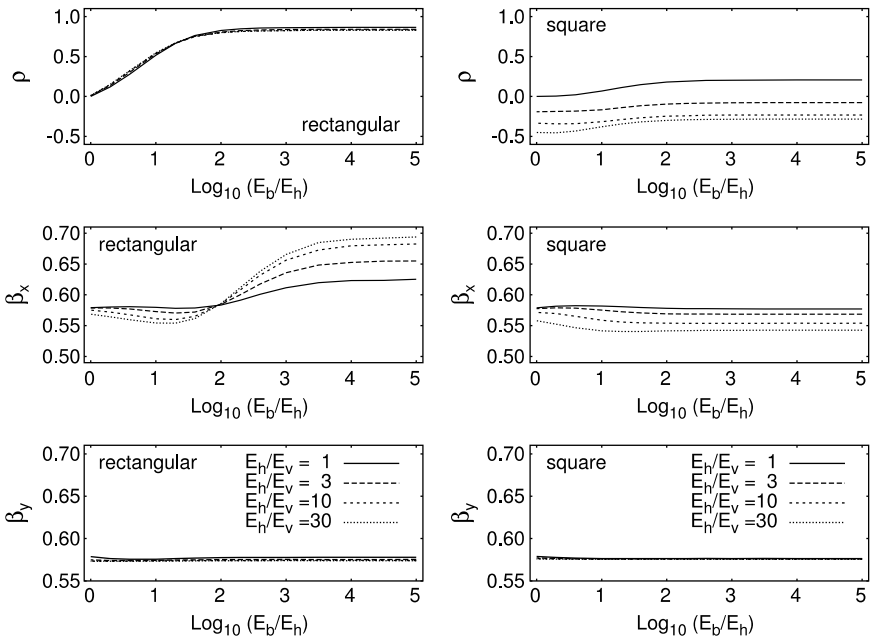

Fig. 13. Trend of the elastic parameters as a function of different ratios E_b/E_h and E_h/E_v for the textures with rectangular blocks (left), and square blocks (right).

E_b/E_h ratio. For the present two textures, characterized by continuous horizontal mortar joints, the micro-structure does not give additional bending stiffness along the vertical direction and parameter β_y always remains centred around value 0.577.

The results of this linear-elastic identification can be put into relation with a numerical analysis that considers the elastic–plastic behaviour of mortar. To do this, a plane stress finite element model was used for analyses in which the bricks were linear elastic, while the mortar behaviour followed the linear Drucker–Prager plasticity material model available within Abaqus code. In the examples shown in Fig. 14, the initial Young's moduli were assigned to be $E_b = E_h = 10000$ MPa, while the weakness effect of the vertical mortar joints was investigated by considering the same four E_h/E_v ratios already mentioned. The yield surface was non-circular in the deviatoric plane with a ratio of the flow stress in triaxial tension to the flow stress in triaxial compression equal to $K = 0.78$, and a non-associated flow was assumed with separate dilatation (2°) and friction (30°) angles in the "meridional" stress plane (Hibbitt et al., 2002). First yield occurred at a value of cohesion $d = 2$ MPa, that corresponded to a yield stress in pure shear equal to $\tau = 2Kd/(\sqrt{3}(1+K)) = 1.01$ MPa. The horizontal mortar joints material then hardened to $d = 2.2$ MPa at one percent strain, and again to $d = 2.4$ MPa at ten percent strain. The strength ratio of the horizontal and vertical mortar joints was the same as the stiffness ratio. Fig. 14 shows in particular the trends of ratio ρ as a function of the average shear strain ε_s during monotonic shear loading under periodic boundary conditions. The graphs of the average shear stress τ_s show how the quality of the vertical mortar joints significantly affects the global shear strength for the square block texture, while in the case of rectangular blocks the micro-structure effect of the texture somehow tends to compensate the vertical joint weakness.

The evolution trend of the local rotation ratio ρ during an elastic–plastic loading can easily be modelled with the present rigid elements by identifying suitable constitutive-laws for vertical and horizontal shear connection devices, as shown in the two examples of Fig. 15. In particular, the behaviour of the rectangular block texture is approximated by giving the vertical shear connection a strength and a post-elastic stiffness

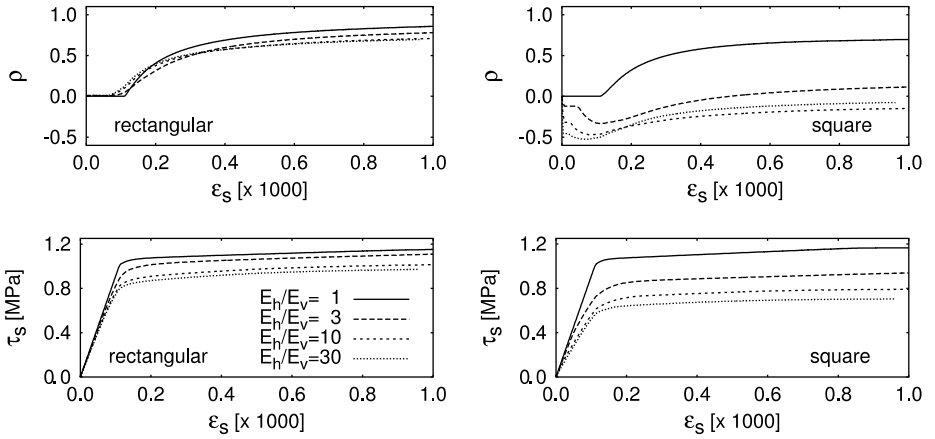

Fig. 14. Local rotation and average shear stress as a function of mean shear strain using finite elements with a linear Drucker–Prager plasticity material model for mortar.

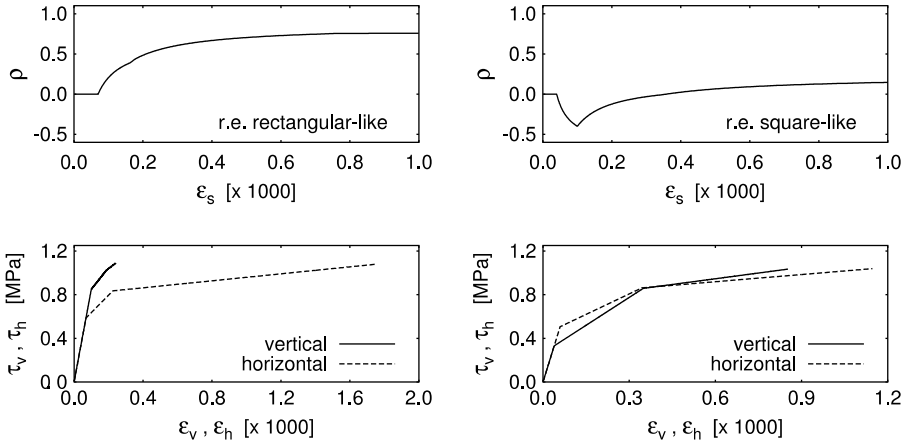

Fig. 15. Examples of the evolution of local rotation ratio ρ as a consequence of different constitutive laws $(\varepsilon - \tau)$ assigned to the vertical and horizontal shear springs of rigid elements.

higher than the horizontal connections. On the other hand, the behaviour of the square block texture is approximated by assigning a substantially similar behaviour to the two shear connections.

4.3. Comparisons with finite elements

The performance of the present model is presented by comparing the results of a set of eigenvalue studies carried out on simple square structures. Figs. 16 and 17, in particular, refer to the first eigen-solution calculated by means of four numerical models: a composite finite element model that was assumed as reference, a rigid element model with shear springs defined according to Eq. (9) and distances b_x and b_y defined according to Eq. (12) (“full r.e.”), a rigid element model with symmetric shear stiffness ($\rho = 0$, “symm r.e.”), and a finite element model that adopts an orthotropic homogeneous Cauchy material (“homogeneous f.e.”). A fixed vertical left side was considered as a boundary condition, as it has more

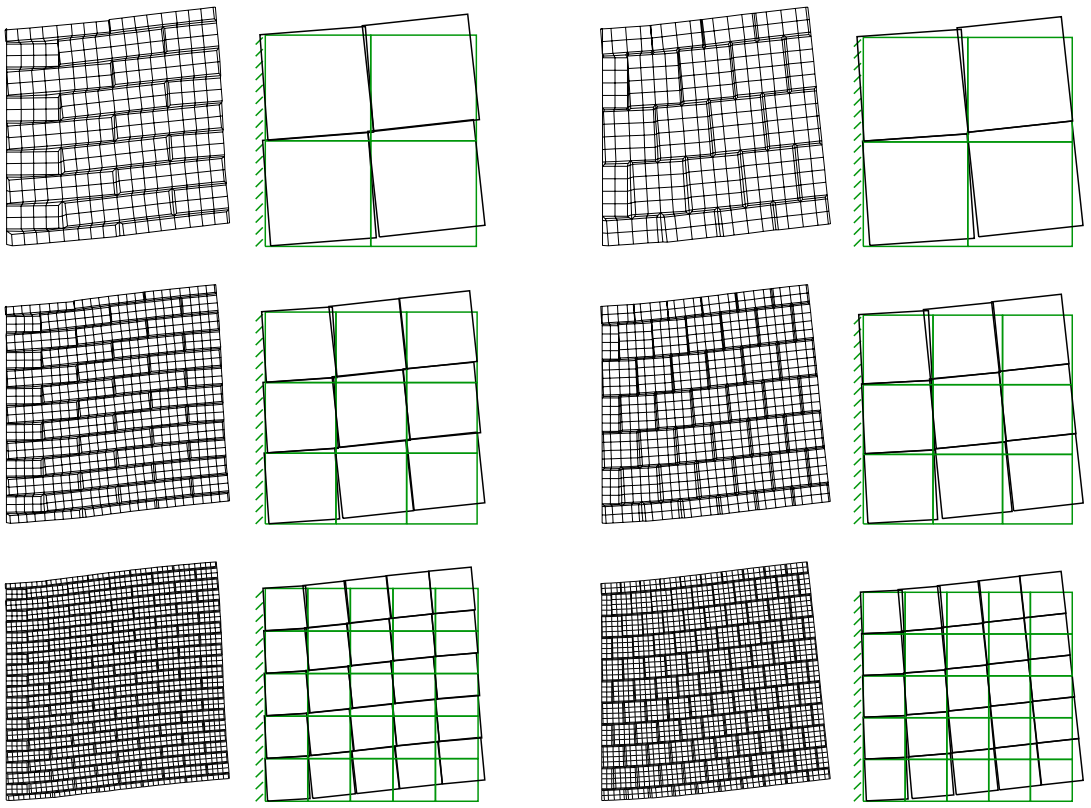

Fig. 16. Comparison of the deformed shapes corresponding to the first eigenvalue for different composite structures 2×2 (top), 3×3 (middle), 5×5 (bottom), with rectangular and square block textures; $E_b/E_h = 100$, $E_h/E_v = 10$.

evident micro-structure effects, and a ratio of about 1/100 was chosen among the number of degrees of freedom of the two approaches as reported in Table 1. It must be noted that further refinements of the rigid element meshes do not make sense in these cases because the element size already corresponds to that of the periodic cell adopted for identification.

A qualitative confirmation of the capability of the present approach to catch the "memory" of different textures is obtained by observing the rigid element deformed shapes of Fig. 16. In fact, the vertical connection sides of the rigid elements that correspond to rectangular block textures show a marked terraced disposition, while they are almost aligned when the elements correspond to the cases of square block textures. Logically, this effect is less pronounced when the size of the blocks is small with respect to the global size of the structure as evident in the 5×5 case.

The graphs of percentage errors $\Delta\omega\%$ in the computation of the first eigenvalue with respect to the composite finite element model, as shown in Fig. 17, reveal that, for square block textures, the approximation is good and substantially insensitive to the adopted particular computational model. On the other hand, in the case of rectangular block textures, the capability of dealing with micro-structure effects significantly depends on the different discrete models. In particular the rigid element model with the connection devices defined according to Eqs. (9) and (12) ("full r.e.") has a good performance in the whole range of E_b/E_h ratio, while the finite element model that adopts the orthotropic homogeneous Cauchy material ("homogeneous f.e.") shows a lack of rigidity for high E_b/E_h ratio values. An analogous shortcoming is also manifested by rigid elements when adopting equal shear springs on different sides

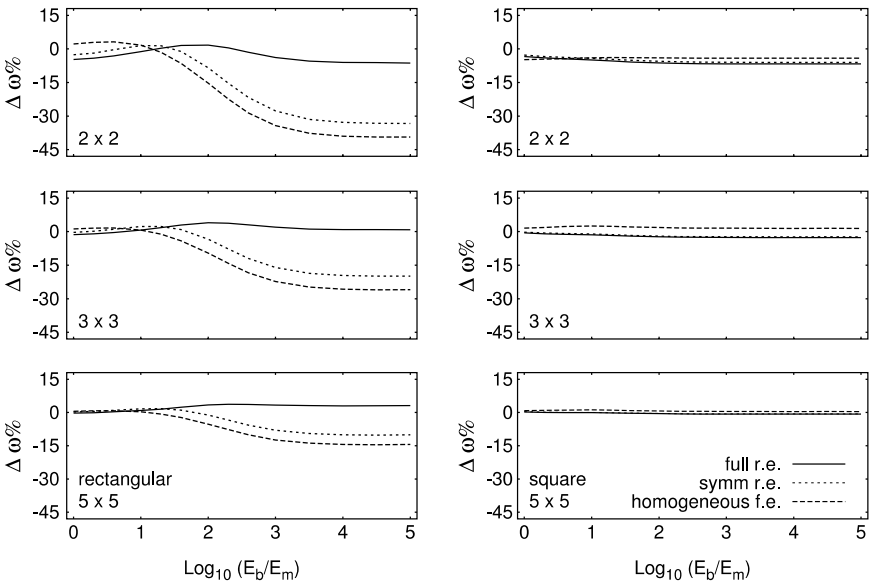

Fig. 17. Evaluation errors of the first eigenvalue with reference to the finite element model of composite textures; $E_h/E_v = 10$.

Table 1
Comparison of the number of degrees of freedom of the finite element models and the rigid element model adopted for the eigenvalue analysis

	Composite finite elements	Specific rigid elements	Homogeneous finite elements
2×2	1242	12	1250
3×3	2726	27	1250
5×5	7422	75	1250

("symm r.e."). The comparison of the plots relating to the 2×2, 3×3 and 5×5 structures also highlights that errors depend on the ratio between the size of rectangular blocks and the global size.

The main source of error of the present method is essentially related to the simple kinematics that assigns only three degrees of freedom to each element. As a consequence, a good performance is expected when analyzing simple structures loaded by inertial body forces that do not produce high strain gradients at the macro-scale, as in the case of the eigenmode I. Figs. 18 and 19 show some other results to appreciate the performance of the present approach when approximating more complex deformation patterns, and also the consequences of employing elements whose size is larger than the periodic cell adopted for elastic identification. In correspondence with the third eigenvalue, for example, Fig. 18 shows the comparison of deformed shapes of 25, 9 and 4 rigid element meshes with respect to the 5×5 composite structure, and it is interesting to note the different local rotation exhibited by the elements depending on the fact that they are approximating the rectangular or the square texture. From the error plots shown in Fig. 19 we see that the level of approximation is sensitive to the refinement of the rigid element meshes. In particular the error curves of 2×2, 3×3, and 4×4 meshes converge toward the error curve of the 5×5 mesh that can be considered a "target" since these elements have the same size of the adopted representative volume element. In any case, it is noticeable that the proposed approach gives good results even with a very coarse mesh of 4 rigid elements in the whole range of E_b/E_h ratio. This fact confirms the effectiveness of Eqs. (15) and (16) in dealing with micro-structure size effects.

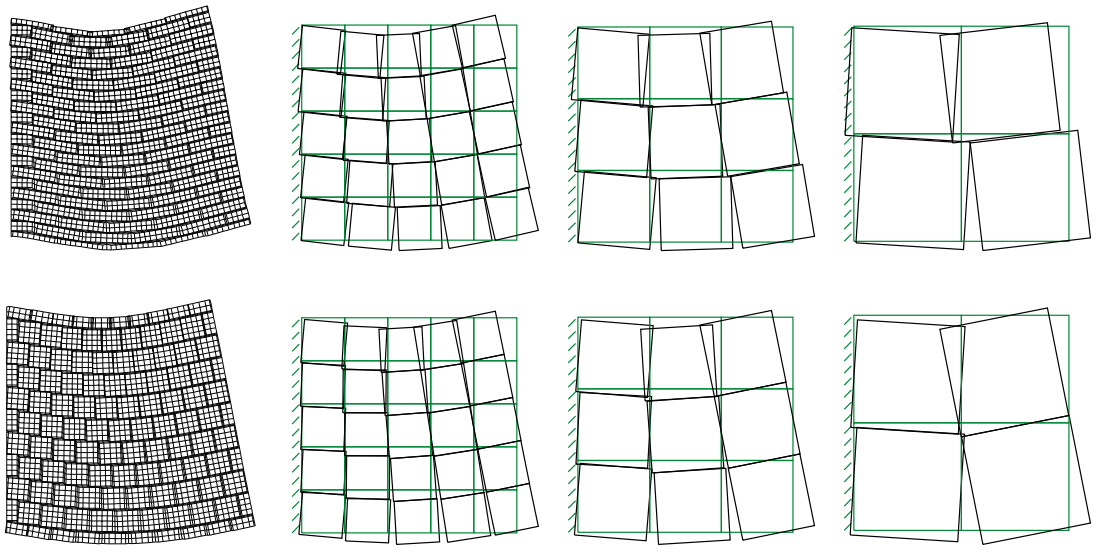

Fig. 18. Comparison of the deformed shapes corresponding to the third eigenvalue of the 5×5 composite structure adopting meshes of 25, 9 and 4 rigid elements for rectangular (top) and square block textures (bottom).

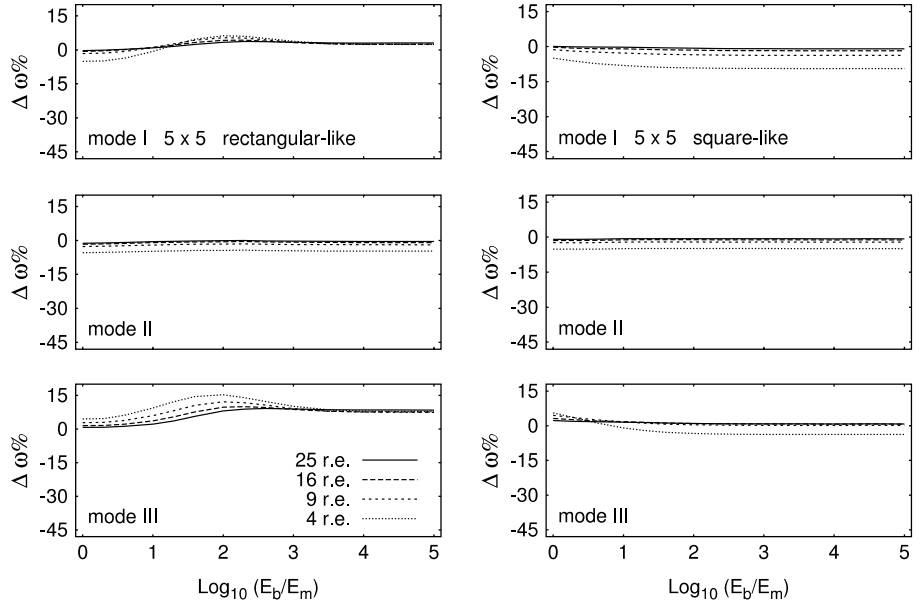

Fig. 19. Error curves for the eigenvalue of modes I–III of the 5×5 structure adopting meshes of 25, 16, 9 and 4 rigid elements for rectangular and square block textures; ratio $E_h/E_v = 10$.

A final example for evaluating distortion effects is given by comparing the results obtained with the four meshes shown in Fig. 20. The graphs with the error plots for the first eigenvalue confirm the good performance of Eqs. (19), (23) and (24) in dealing with distortions. It must be noted that the approximation

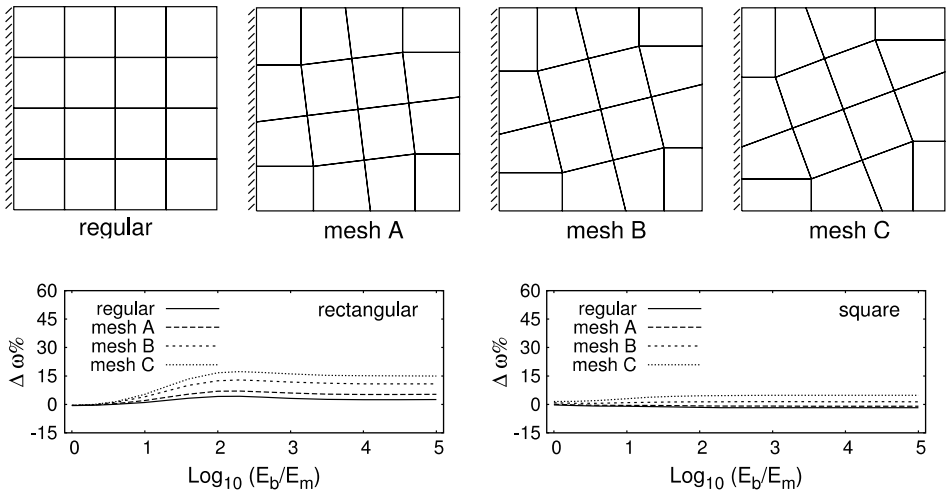

Fig. 20. Meshes adopted for evaluating the effects of distortion (top). Error plots for the first eigenvalue of the "5×5" structure adopting regular and distorted meshes A–C (bottom); ratio $E_h/E_v = 10$.

error always remains moderate and lower than in the case of regular mesh with orthotropic homogeneous Cauchy material shown in Fig. 17.

5. Conclusions

The demand for a computational model that requires very few degrees of freedom to describe the global dynamics of composite masonry-like structures is at the basis of the present approach. Focusing on a level of detail larger than the size of the minimum periodic cell, a direct specific identification procedure has been conceived in order to transfer essential texture information from the composite micro-scale to the rigid element meso-scale. The innovative aspect of the present approach is treating heterogeneous composite material as a structured continuum without involving homogenization towards a generalized Cosserat continuum, and thus avoiding the related complexities in assigning elasticity and plasticity characteristics. This is obtained by completely renouncing the concept of continuum and exploiting the intrinsic characteristics of the kinematics of the rigid elements that can be viewed as a sort of "Cosserat discrete medium".

An extensive numerical investigation has proved that micro-structure effects become particularly relevant for high ratios between the elastic moduli of the constituents, when texture plays an important role giving additional resources of stiffness and strength. The present method has proved successful by assigning to the rigid elements a "memory" of the original texture also when adopting very coarse meshes, and in any case it shows a better performance compared to the adoption of a homogeneous orthotropic Cauchy continuum. The present study is therefore promising in view of the implementation of the post-elastic behaviour of the material.

References

Anthoine, A., 1995. Derivation of the in-plane elastic characteristics of masonry through homogenization theory. International Journal of Solids and Structures 32 (2), 137–163.

Bouyge, F., Jasiuk, I., Ostoja-Starzewski, M., 2001. A micromechanically based couple-stress model of an elastic two-phase composite. International Journal of Solids and Structures 38 (10–13), 1721–1735.

Casolo, S., 1999. Rigid element model for non-linear analysis of masonry façades subjected to out-of-plane loading. Communications in Numerical Methods in Engineering 15 (7), 457–468.

Casolo, S., 2000. Modelling the out-of-plane seismic behaviour of masonry walls by rigid elements. Earthquake Engineering and Structural Dynamics 29 (12), 1797–1813.

Dialer, C., 1991. Some remarks on the strength and deformation behaviour of shear stressed masonry panels under static monotonic loading. In: Proceedings of 9th International Brick Block Masonry Conference. Berlin, pp. 276–283.

Hibbitt, Karlsson & Sorensen, Inc., 2002. ABAQUS Manuals. version 6.3.

Kawai, T., 1978. New discrete models and their application to seismic response analysis of structures. Nuclear Engineering and Design 48, 207–229.

Masiani, R., Rizzi, N., Trovalusci, P., 1995. Masonry as structured continuum. Meccanica 30 (6), 673–683.

Michel, J.C., Moulinec, H., Suquet, P., 1999. Effective properties of composite materials with periodic microstructure: a computational approach. Computer Methods in Applied Mechanics and Engineering 172, 109–143.

Mühlhaus, H.-B., 1989. Application of Cosserat theory in numerical solution of limit load problems. Ingenieur-Archiv 59, 124–137.

Pande, G.N., Liang, J.X., Middleton, J., 1989. Equivalent elastic moduli for unit masonry. Computers and Geotechnics 8, 243–265.

Sulem, J., Mühlhaus, H.-B., 1997. A continuum model for periodic two-dimensional block structures. Mechanics of cohesive-frictional materials 2, 31–46.

Toy, Y., Yoshida, S., 1991. Numerical simulation of nonlinear behaviours of two-dimensional block structures. Computers and Structures 41 (4), 593–603.

Trovalusci, P., Masiani, R., 1999. Material symmetries of micropolar continua equivalent to lattices. International Journal of Solids and Structures 36 (14), 2091–2108.

van der Sluis, O., Vosbeek, P.H.J., Schreurs, P.J.G., Meijer, H.E.H., 1999. Homogenization of heterogeneous polymers. International Journal of Solids and Structures 36 (21), 3193–3214.

Zucchini, A., Lourenço, P.B., 2002. A micro-mechanical model for homogenisation of masonry. International Journal of Solids and Structures 39 (12), 3233–3255.